Research Article | Vol. 28, No. 6 / 16 March 2020 / Optics Express 8257

Optics EXPRESS

Description of spatio-temporal couplings from heat-induced compressor grating deformation

VINCENT LEROUX,[1,2] TIMO EICHNER,[2,*] AND ANDREAS R. MAIER[2,1]

[1] *Deutsches Elektronen-Synchrotron DESY, Hamburg, Germany*
[2] *Center for Free-Electron Laser Science & Department of Physics Universität Hamburg, Hamburg, Germany*
[*] *timo.eichner@cfel.de*

Abstract: High average power high-intensity laser systems can suffer from a heat-induced deformation of the final compressor gratings, which introduces wavefront aberrations and spatio-temporal couplings to the pulse. Here, we use a simple numerical description, that was first introduced by Li *et al.* (Appl. Phys. Express, 10, 102702, 2017 and Optics Express, 26, 8453, 2018), to calculate the resulting degradation of the peak intensity and the 3-dimensional deformation of the laser pulse as a function of average power, and verify the results using experimental data. For a typical 100 TW-class laser we find that non-negligible pulse distortions can occur at an average power as low as 2.7 Watts. An open source implementation of our numerical description is available for researchers to estimate the effects of spatio-temporal couplings for their specific laser configuration.

1. Introduction

High peak power TW-class lasers have become an indispensable tool in a large range of applications, such as particle acceleration, high-energy physics, or warm dense matter studies [1,2]. These lasers are typically based on a chirped-pulse amplification (CPA) architecture and often use the large bandwidth supported by Ti:Sapphire crystals to achieve the few-femtosecond pulse lengths required for highest intensities.

Irregularities in the dispersive sections of the laser can introduce spatio-temporal couplings (STC), such as spatial chirp, pulse front tilt or pulse front curvature [3]. When under control, STCs become a very powerful tool to finely adjust some experimental parameters. For example, spatial chirp has been used for simultaneous spatial and temporal focusing, which has applications in multiphoton microscopy [4]. Pulse front tilt allows to steer electron bunches generated by laser-plasma wakefield acceleration [5]. Pulse front curvature used in combination with temporal chirp leads to a "flying focus", which couples the position and evolution of the laser peak intensity [6,7].

However, when they are not controlled, spatio-temporal couplings can be detrimental to experiments, as they decrease the available peak intensity in focus. Furthermore, both the pulse duration and the spatial extent of the pulse are asymmetrically increased, causing a very complex propagation of the pulse through the focal plane [8]. Those asymmetries of the pulse shape are, in particular, very difficult to model in particle-in-cell simulations supporting laser-plasma acceleration, causing significant discrepancies between simulations and experimental results.

A main source of STCs is the laser pulse compressor as it uses angular dispersion to change the group delay dispersion of the whole beam. A misalignment of the compressor will result in STCs for the output beam [9]. A surface deformation of the compressor optics in general will result in higher order STCs, which are especially difficult to correct [10–12]. The final compressor gratings in particular are a common source of STCs, since they typically feature a gold coating to support sufficient bandwidth for ultrashort pulses. While gold-coated optics do support large bandwidths,

#386112 https://doi.org/10.1364/OE.386112
Journal © 2020 Received 18 Dec 2019; revised 13 Feb 2020; accepted 18 Feb 2020; published 6 Mar 2020

Optics EXPRESS

they have the disadvantage that a small percentage of the incident laser power is absorbed by the coating and thus the substrate. As the compressor is set up in a vacuum environment the heat cannot be removed efficiently. Depending on the substrate's coefficient of thermal expansion (CTE), the local heating introduced by the laser causes a deformation of the substrate. For high average power lasers, this effect can result in a drastic degradation of the pulse quality. Previous work reported this issue [13–15], but focused on the spectrum-averaged wavefront degradation. The measurement of the heat-induced degradation of the spectrally integrated wavefront, as it was done by Leroux [14] and Clady [15], underestimates the deterioration of focal intensity and has to be extended to include spatio-spectral effects for a complete illustration of the problem.

Here, we use the model introduced by Li *et al.* [11,12] to study the spatio-temporal couplings resulting from thermally induced deformation of the final compressor gratings in a TW-class CPA laser, and to understand the effects of these couplings on the available peak intensity. We provide a numerical implementation of this formalism as open source code, and benchmark the code with experimental data previously reported [14]. The code is easy to use and will allow researchers to estimate the effects of heat-induced grating deformation for their specific laser system.

This paper is structured as follows. First, we describe the formalism introduced by Li *et al.* [11,12] that allows us to calculate the 3D laser pulse shape from deformations of the optics. Then, we use the parameters of our laser system to showcase the change of the main beam properties and the STCs in the focal plane as a function of average power in the compressor. We validate our description using measured pulse properties. Finally, we draw conclusions on the optimum average power of the laser beam to reach the maximum peak intensity in focus. While the calculations reported here are specific to our laser system, it is straightforward to adapt them to other laboratories and facilities operating at similar laser average powers.

2. Methods

Gold-coated compressor gratings typically used in Ti:Sapphire lasers absorb a few-percent fraction of the incident laser power, causing a localized thermal expansion and thus deformation of the grating substrates. Depending on the substrate material, this effect can cause significant spatio-temporal couplings in the pulse. In order to estimate this impact, we first simulate the deformation profile of the gratings surface. Then, we use this profile to calculate a frequency dependent wavefront that is added to the the input laser electric field, as it was described in Li *et al.* [11,12]. Finally, using Fourier transformations, we estimate the 3D spatio-temporal profile of the pulse in the focal plane.

2.1. Grating deformation

By simulating the grating deformation from the absorbed heat, we aim to reproduce the measured results of our previous experiment reported in [14]. Therefore, we use the same laser system parameters (see Table 1) which are typical for modern 100 TW-class systems. The maximum energy sent into the compressor is 6 J, at a repetition rate of 5 Hz, which leads to a maximum average power of 30 W. The near field intensity profile is a 6^{th} order super-Gaussian profile with a 70 mm full width at half-maximum (FWHM). In order to focus on the aberrations introduced by thermal effects, static wavefront errors of the beam or the diffraction gratings are not considered. The holographic gratings consist of a gold-coated Pyrex substrate with a groove density of 1480 lines/mm, and are operated at an incidence angle of 51.4°. The two gratings are used in a double pass configuration, and therefore a fraction of the laser beam is absorbed twice at each grating. Additionally, the grating diffraction efficiency was measured to be 92 % and this value is used to decrease the laser energy after each pass. A Gaussian spectrum with a FWHM bandwidth of 32 nm was used for the simulations.

Using these parameters, we simulate the deformation profile of the grating substrate with the COMSOL Multiphysics thermal expansion module for different laser average powers ranging

Optics EXPRESS

Table 1. Parameters of the ANGUS laser system that were used as an input for the simulations presented in this work. These parameters are typical for a Ti:Sapphire 100-TW class laser system.

Pulse energy before compressor	6 J
Pulse repetition rate	5 Hz
Fourier limited pulse duration (FWHM)	29 fs
Near field intensity profile	6^{th} order super-Gaussian
Beam diameter (FWHM)	70mm
Angle of incidence on compressor gratings	51.4°
Groove density of compressor gratings	1480 lines/mm
Grating diffraction efficiency	92%
Coating absorption	3.6%

from 0 W (no deformation) to 30 W (maximum deformation), with radiative cooling of the laser substrates. To be able to compare the results to measurements, we use the same 30 minutes of laser exposure as in our previous experiment [14], where we found that most of the deformation occurs before this time scale.

In those measurements, we observed that the average divergence of the beam θ_{avg} at the exit of the compressor depends on the average power incident on the gratings P_{in} such that θ_{avg} [µrad] = $2.9 \times P_{\text{in}}$[W]. Therefore, we scale the simulated absorption of the gold coating such that the output beam divergence matches the measurement. We obtain an absorption of 3.6 %, which is in good agreement with the 3.75 % calculated from the complex refractive index for an 800 nm wavelength and a flat vacuum-gold interface at an angle of incidence of 51.4° [16,17].

Figure 1 shows the deformation profile simulated for the second grating at the maximum average power (30 W). We call the deformation profiles of the two gratings $d_{\text{G1}}(x_{\text{gr}}, y)$ and $d_{\text{G2}}(x_{gr}, y)$, with the horizontal coordinate x_{gr} in the plane of the grating surface and y, the vertical coordinate.

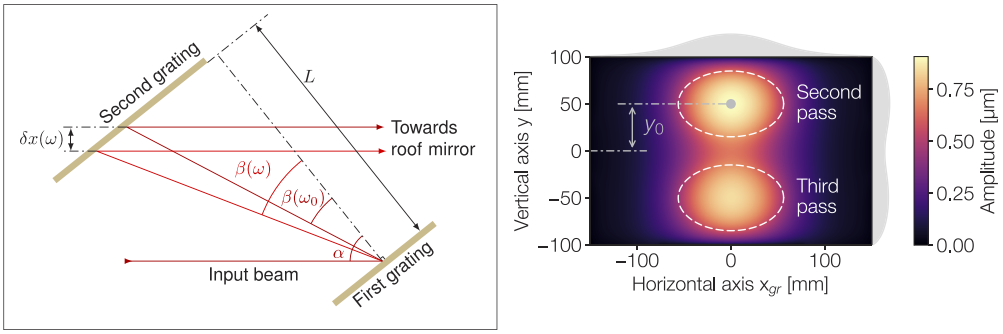

Fig. 1. The compressor layout with the notation used in the text (left), and the deformation profile of the second grating normal to the surface d_{G2} simulated with COMSOL. Simulations show the deformation after 30 minutes of laser operation at 30 W average power. The full width at half maximum of the second and third passes of the compressor are indicated in white dashed line. The shaded areas show the projected deformation profile.

Following [12], we introduce the projected deformation profiles $f_{\text{G1}}(x, y, \omega)$ and $f_{\text{G2}}(x, y, \omega)$ that are imprinted onto the laser wavefront as the pulse is diffracted on the grating surface. Here, x denotes the horizontal coordinate in the reference frame of the wavefront. These profiles represent the transversely resolved difference in path length that is caused by the bulging of the

Optics EXPRESS

grating surface. To calculate them, we project the deformation profiles of the gratings to the plane of the laser wavefront. The projection consists of a scaling of a) the horizontal axis $x = x_{\mathrm{gr}} \cos\alpha$ of the grating according to the angle of incidence, and b) the amplitude of the deformation, to account for the fact that the deformation profiles d_{G1} and d_{G2} are normal to the grating surface and not along the direction of propagation:

$$f_{\mathrm{G1,\,G2}}(x, y, \omega) = \left[\frac{1}{\cos\alpha} + \frac{1}{\cos\beta(\omega)}\right] d_{\mathrm{G1,\,G2}}(x_{\mathrm{gr}}\ \cos\alpha, y) \tag{1}$$

Here, α is the angle of incidence on the gratings and $\beta(\omega)$ is the frequency dependent angle of diffraction, as is illustrated in Fig. 1. The wavefront aberration after each pass f_i can then be expressed as:

$$\begin{aligned} f_1(x,\ y) &= f_{\mathrm{G1}}(x,\ y - y_0,\ \omega),\\ f_2(x,\ y,\ \omega) &= f_{\mathrm{G2}}(x + \delta x(\omega),\ y - y_0,\ \omega),\\ f_3(x,\ y,\ \omega) &= f_{\mathrm{G2}}(x + \delta x(\omega),\ -y - y_0,\ \omega),\\ f_4(x,\ y) &= f_{\mathrm{G1}}(x,\ -y - y_0,\ \omega), \end{aligned} \tag{2}$$

with y_0 the vertical offset from the center of the grating, and $\delta x(\omega)$ the frequency-dependant horizontal shift of a frequency ω on the second grating with respect to the central frequency ω_0. This shift can be written as:

$$\delta x(\omega) = (\tan\beta(\omega_0) - \tan\beta(\omega))\ \cos\alpha\ L, \tag{3}$$

with β the diffraction angle, α the angle of incidence, and L the distance between the two gratings along the normal. We note that for the last two passes, the vertical axis is flipped, as our setup features a roof mirror.

2.2. Spectro-spatial phase

For a compressor with a negligible change of beam properties during the propagation between the gratings, we can then write the total, frequency-resolved wavefront deformation $\phi_{\mathrm{comp.}}$ added to the beam by the deformed compressor gratings as

$$\phi_{\mathrm{comp.}}(x, y, \omega) = k(\omega)\,[f_1(x, y, \omega) + f_2(x, y, \omega) + f_3(x, y, \omega) + f_4(x, y, \omega)] \tag{4}$$

with the wave vector amplitude $k(\omega)$.

For an arbitrary input pulse $E_{\mathrm{NF},\,in}(x, y, \omega) = A(x, y, \omega)e^{i\,\phi_0(x,y,\omega)}$, with an envelope $A(x, y, \omega)$ and an initial phase $\phi_0(x, y, \omega)$, we can now calculate the effect of the compressor by adding the phase term to the initial pulse:

$$E_{\mathrm{NF,\,out}}(x, y, \omega) = E_{\mathrm{NF,\,in}}(x, y, \omega)\ e^{i\,\phi_{\mathrm{comp.}}(x,y,\omega)}. \tag{5}$$

To calculate the beam properties of the pulse in the focus, we neglect a longitudinal shift of the focal plane and a detuning of the group delay dispersion (GDD) of the compressor that are caused by the deformation of the gratings. To do this, we first remove the frequency-averaged spherical curvature of the wavefront, which simply corresponds to the divergence of the beam, and thus a longitudinal shift of the focal plane. The curvature is determined through a parabolic fit to the frequency-averaged phase of the electric field. This resulting divergence is reported in Fig. 3(a), where we compare it to the measured laser divergence. The GDD is determined from the quadratic component of the spectral phase on the beam axis and is removed from the pulse to mimic a compressor that is tuned for optimal compression. Then, by performing a 2D Fourier

Optics EXPRESS

transform for each frequency, we obtain the focal spot in the space-frequency domain

$$E_{\mathrm{FF}}(\xi,\eta,\omega) = FT_2\left[E_{\mathrm{NF,\,out}}(x,y,\omega)\right]. \tag{6}$$

In the focus η and ξ denote the vertical and horizontal coordinates. Finally, an inverse Fourier transform at each spatial position gives the 3D spatio-temporal focal spot

$$E_{\mathrm{FF}}(\xi,\eta,t) = iFT\left[E_{\mathrm{FF}}(\xi,\eta,\omega)\right], \tag{7}$$

from which we can derive the relevant information such as peak intensity, pulse duration, waist, but also pulse front tilt, or spatial chirp for instance.

Apart from the COMSOL simulation, this whole calculation is implemented in Python language and available as open source [18].

3. Results

For the following calculations we use the Angus laser parameters, as reported above. At the maximum average power, the deformation of the grating surface over the area of the laser leads to 0.9 λ peak-to-peak of wavefront deformation (compare Fig. 1) and consequently to a severe degradation of the focus quality. The near field profile is focused by an optic with a focal length of 2 meters, which corresponds to the setup of the laser-plasma accelerator Lux [19]. We therefore compare the pulses in the focal plane of this setup for an average power of 0 W (no deformation), and 30 W (maximum deformation). Please refer to Visualization 1 for an animation of the 3-dimensional laser pulse shape in focus as a function of average power.

Figure 2 shows the integrated profiles of these two extreme cases. There is a strong pulse front tilt in the horizontal plane, which amounts to 0.83 fs/μm. The spatial profile is distorted by $\lambda/3$ of

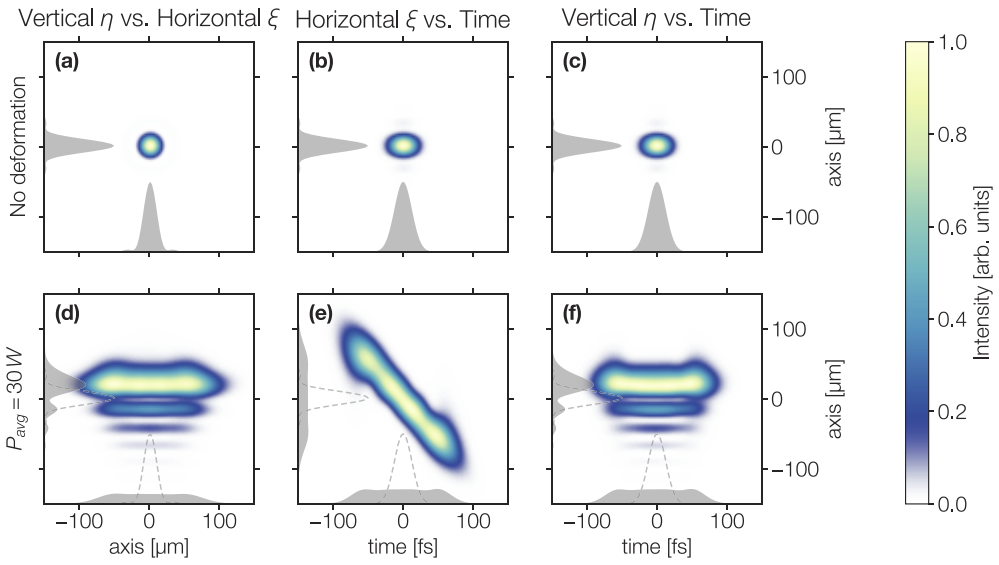

Fig. 2. Integrated horizontal-vertical (a, d), horizontal-temporal (b, e), and vertical-temporal (c, f) profiles, with no deformation (a–c), and with a 30 W average power deformation (d–f). One can see a strong wavefront deformation in the vertical plane, and a strong pulse front tilt and spatial chirp in the horizontal plane. The shaded areas show the respective projections, and the dashed lines show the projections of the Fourier limited focal spot. The initial beam size $\omega_{\mathrm{x,y}}$ is 25.5 μm in both planes and the pulse duration is 29.5 fs

Optics EXPRESS

astigmatism at 0°, $\lambda/24$ of coma at 90°, and $\lambda/19$ of trefoil at 90°(all values are rms amplitude). Furthermore, the focal spot is broadened in the horizontal axis by spatial chirp, which amounts to approximately 0.52 mm/(rad·fs^{-1}) for the maximum average power. We do not observe any significant higher order STC, such as pulse front curvature.

Following the notation of [20], we write the pulse front tilt p such that $E(x,t) = E_x(x)E_t(t-p\cdot x)$, and the spatial chirp ζ such that $E(x,\omega) = E_x(x-\zeta\cdot\omega)E_\omega(\omega)$.

Figure 3 shows the evolution of the main laser spatio-temporal properties, namely the divergence of the beam in the near field (which we remove before simulating the focal spot as explained above), the time integrated waist, the space integrated pulse duration, the horizontal spatial chirp, the horizontal pulse front tilt, and the peak intensity normalized to the non-deformed focal spot peak intensity. We observe that the divergence of the beam matches well with the divergence reported in [14] and are therefore confident, that our code provides a reasonable estimate of the in-focus STCs, even though we could not measure them directly with our experimental layout.

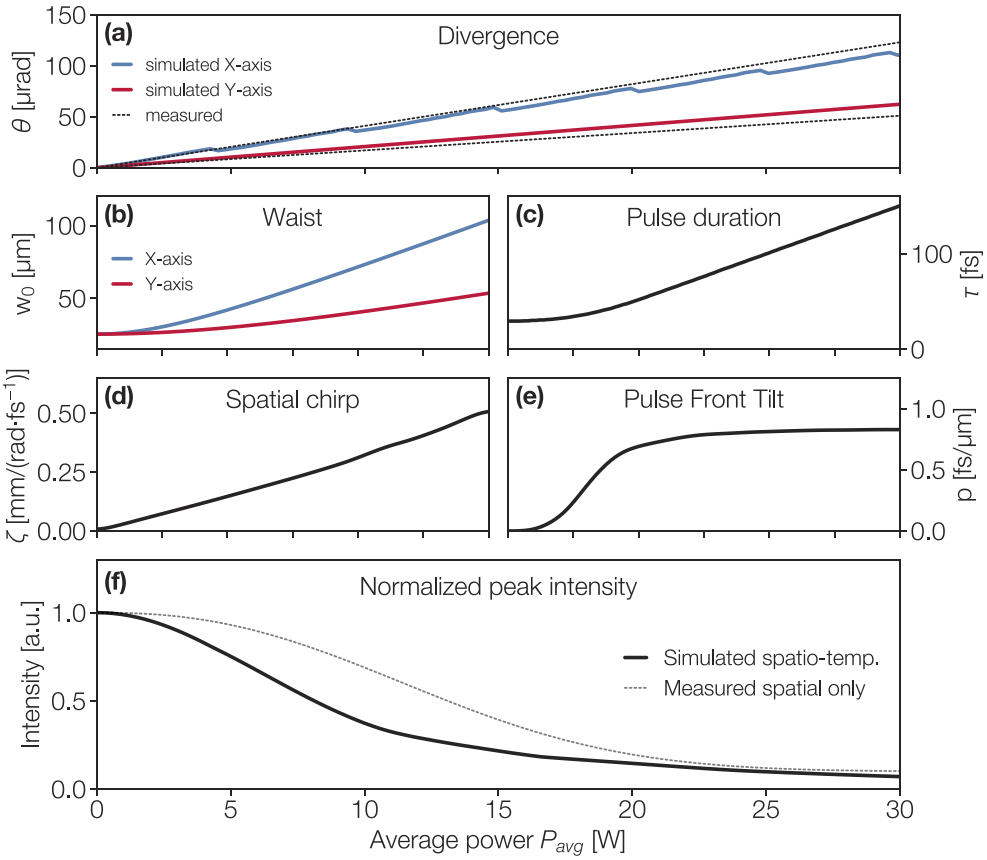

Fig. 3. Evolution of the main laser beam parameters as a function of the laser average power ranging from 0 W to 30 W. Divergence at the exit of the compressor (a) and waist in focus (b) are shown in the horizontal and vertical axes. The waist is integrated over time, and the pulse duration in focus (c) is integrated over the spatial dimensions. The spatial chirp (d) and pulse front tilt (e) correspond to STCs in the horizontal axis. The simulated peak intensity (f, solid) is compared to the measured Strehl ratio [14] (dotted). The step-like variation of the horizontal divergence in (a) is attributed to numerical errors of the simulation.

The spatial chirp scales linearly with the average power, following $\zeta[\mu\text{m}/(\text{rad}\cdot\text{fs}^{-1})] = 16.7 \times P$ [W]. The pulse front tilt stays almost constant above an average power of 11 W. Above this

Optics EXPRESS

value, the focal spot grows at similar rates in time, as well as in the horizontal plane, due to spatial chirp. As a consequence, the two effects are balancing out the growth of the pulse front tilt. Finally, we observe that the spatio-temporal couplings decrease the available peak intensity even further compared to our previous measurements [14], which were limited to the Strehl ration as a time integrated property, and thus did not consider the change in pulse length.

Using these simulations, we calculate that the maximum peak intensity is reached for an average power of 7.1 W (see Fig. 4). At this power, the laser energy contained in the pulse balances with the deformation of the gratings. The peak intensity is still 42 % lower compared to a pulse generated by a non-distorted compressor, and the focal spot features a pulse front tilt of 0.52 fs/µm. For comparison, the projected beam profiles at this optimal average power are shown in Fig. 5. Below an average power of 2.7 W, the pulse front tilt stays negligible and the peak intensity is decreased by only 6.7 % due to the spatial chirp.

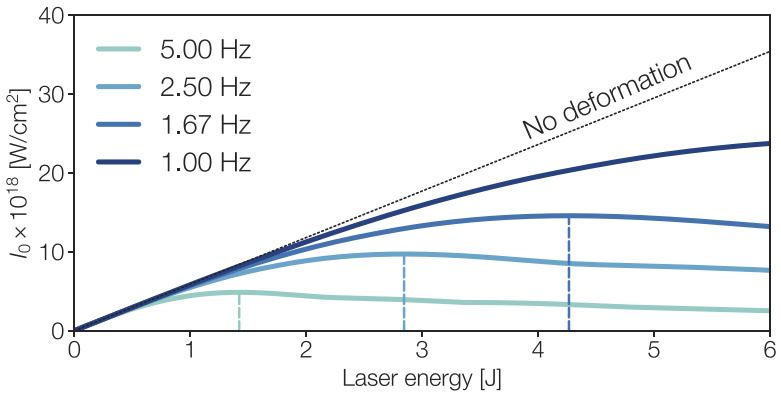

Fig. 4. Simulated peak intensity in focus for different repetition rates. We observe that the peak intensity reaches its maximum for an average power of 7.1 W. At this power, the peak intensity is 42 % lower than the ideal peak intensity with no grating deformation, and there is a pulse front tilt of 0.52 fs/µm.

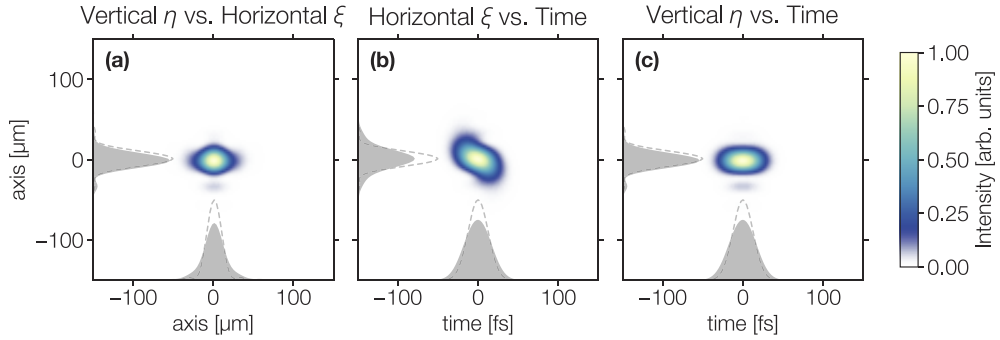

Fig. 5. Integrated horizontal-vertical (a), horizontal-temporal (b), and vertical-temporal (c) profiles, with a 7.1 W average power deformation. The shaded areas show the respective projections, and the dashed lines show the projections of the Fourier limited focal spot.

4. Conclusion

We report on the spatio-temporal couplings resulting from a thermally induced deformation of gold-coated Pyrex-based compressor gratings in a Ti:Sapphire 100 TW-class laser. The

Optics EXPRESS

deformation was simulated using an FEM software to model the heat-induced deformation of the compressor gratings and combined with a custom code to determine the frequency-dependent wavefront of the beam at the output of the compressor. After computing the 3D spatio-temporal beam profile in focus that is visible in Visualization 1, we could derive the evolution of the main beam properties as function of the laser average power. We observe that the main STCs present in the focused beam are spatial chirp and pulse front tilt, i.e., first order couplings. This observation may change in the presence of an intensity modulation of the beam profile, that can lead to a non-uniform deformation in the grating substrate if the thermal gradients are not evened out by thermal diffusion.

We found that there is an optimal average power, at which a maximal peak intensity is reached due to a balancing of the degradation of the spatio-spectral phase of the pulse with an increase in pulse energy. The precise value of this optimal power is highly dependent on the compressor setup. A layout with a larger ratio between beamsize and spatial displacement on the second grating would be less sensitive to the introduction of aberrations of the spatio-spectral phase and would therefore lead to an increased optimal power. In typical laser systems, the relevant parameters such as the grating separation, groove density and beamsize are however difficult to change and a mitigation of the deformation is the preferred choice.

For our specific laser, we calculate that the maximum peak intensity is achieved for an average power of 7.1 W, where the increase of the pulse energy balances the deformation of the gratings and thus the distortion of the focal spot. However, experiments such as laser plasma acceleration, which are very sensitive to pulse front tilt and spatial chirp, have to be operated at even lower average powers. This is a significant result, as our specifications and operation parameters can be considered as representative for a number of similar TW-class lasers and will gain importance as a next generation of high average power ultrafast lasers is being developed. The numerical implemetation in Code 1 [18] provides a simple tool for researchers to model and predict STCs for a specific laser setup.

Already at an average power of a few Watt, the heating of the grating substrates through absorption in the gold coating exceeds the radiative cooling. Without active cooling [13], the compressor will not reach a thermal equilibrium, thus preventing reliable long-term operation of the laser.

To mitigate the detrimental effects of STCs in high average power lasers at least on a short time scale, compressors should be built from low-CTE substrates such as fused silica, or ultra-low expansion glass. For our system, we find significant improvements for a compressor based on fused silica grating substrates, and expect even better performance in the future using ultra-low expansion glass. A laser driving applications sensitive to focal quality should also include techniques to pre-compensate and actively control the beam quality. While distortions of the spectrally integrated wavefront can be compensated with a deformable mirror, more sophisticated techniques have to be implemented to pre-compensate spatio-temporal couplings [21].

Funding

Deutsches Elektronen-Synchrotron; Universität Hamburg; Bundesministerium für Bildung und Forschung (05K16GU2).

Acknowledgments

The authors acknowledge M. Kirchen and S. Jalas (UHH) for useful discussions.

Disclosures

The authors declare no conflicts of interest.

Optics EXPRESS

References

1. C. N. Danson, C. Haefner, J. Bromage, T. Butcher, J.-C. F. Chanteloup, E. A. Chowdhury, A. Galvanauskas, L. A. Gizzi, J. Hein, D. I. Hillier, N. W. Hopps, Y. Kato, E. A. Khazanov, R. Kodama, G. Korn, R. Li, Y. Li, J. Limpert, J. Ma, C. H. Nam, D. Neely, D. Papadopoulos, R. R. Penman, L. Qian, J. J. Rocca, A. A. Shaykin, C. W. Siders, C. Spindloe, S. Szantmári, R. M. G. M. Trines, J. Zhu, P. Zhu, and J. D. Zuegel, "Petawatt and exawatt class lasers worldwide," High Power Laser Sci. Eng. **7**, e54 (2019).
2. G. A. Mourou, T. Tajima, and S. V. Bulanov, "Optics in the relativistic regime," Rev. Mod. Phys. **78**(2), 309–371 (2006).
3. S. Akturk, X. Gu, P. Bowlan, and R. Trebino, "Spatio-temporal couplings in ultrashort laser pulses," J. Opt. **12**(9), 093001 (2010).
4. G. Zhu, J. van Howe, M. Durst, W. Zipfel, and C. Xu, "Simultaneous spatial and temporal focusing of femtosecond pulses," Opt. Express **13**(6), 2153–2159 (2005).
5. A. Popp, J. Vieira, J. Osterhoff, Z. Major, R. Hörlein, M. Fuchs, R. Weingartner, T. P. Rowlands-Rees, M. Marti, R. A. Fonseca, S. F. Martins, L. O. Silva, S. M. Hooker, F. Krausz, F. Grüner, and S. Karsch, "All-optical steering of laser-wakefield-accelerated electron beams," Phys. Rev. Lett. **105**(21), 215001 (2010).
6. A. Sainte-Marie, O. Gobert, and F. Quéré, "Controlling the velocity of ultrashort light pulses in vacuum through spatio-temporal couplings," Optica **4**(10), 1298–1304 (2017).
7. D. H. Froula, D. Turnbull, A. S. Davies, T. J. Kessler, D. Haberberger, J. P. Palastro, S.-W. Bahk, I. A. Begishev, R. Boni, S. Bucht, J. Katz, and J. L. Shaw, "Spatiotemporal control of laser intensity," Nat. Photonics **12**(5), 262–265 (2018).
8. K. Nakamura, H. S. Mao, A. J. Gonsalves, H. Vincenti, D. E. Mittelberger, J. Daniels, A. Magana, C. Toth, and W. P. Leemans, "Diagnostics, control and performance parameters for the BELLA high repetition rate petawatt class laser," IEEE J. Quantum Electron. **53**(4), 1–21 (2017).
9. K. Osvay, A. P. Kovacs, Z. Heiner, G. Kurdi, J. Klebniczki, and M. Csatari, "Angular dispersion and temporal change of femtosecond pulses from misaligned pulse compressors," IEEE J. Sel. Top. Quantum Electron. **10**(1), 213–220 (2004).
10. J. Qiao, J. Papa, and X. Liu, "Spatio-temporal modeling and optimization of a deformable-grating compressor for short high-energy laser pulses," Opt. Express **23**(20), 25923–25934 (2015).
11. Z. Li, K. Tsubakimoto, H. Yoshida, Y. Nakata, and N. Miyanaga, "Degradation of femtosecond petawatt laser beams: Spatio-temporal/spectral coupling induced by wavefront errors of compression gratings," Appl. Phys. Express **10**(10), 102702 (2017).
12. Z. Li and N. Miyanaga, "Simulating ultra-intense femtosecond lasers in the 3-dimensional space-time domain," Opt. Express **26**(7), 8453–8469 (2018).
13. D. A. Alessi, P. A. Rosso, H. T. Nguyen, M. D. Aasen, J. A. Britten, and C. Haefner, "Active cooling of pulse compression diffraction gratings for high energy, high average power ultrafast lasers," Opt. Express **24**(26), 30015–30023 (2016).
14. V. Leroux, S. W. Jolly, M. Schnepp, T. Eichner, S. Jalas, M. Kirchen, P. Messner, C. Werle, P. Winkler, and A. R. Maier, "Wavefront degradation of a 200 TW laser from heat-induced deformation of in-vacuum compressor gratings," Opt. Express **26**(10), 13061–13071 (2018).
15. R. Clady, Y. Azamoum, L. Charmasson, A. Ferré, O. Utéza, and M. Sentis, "22 W average power multiterawatt femtosecond laser chain enabling 10^{19}W/cm^2 at 100 Hz," Appl. Phys. B **124**(5), 89 (2018).
16. P. B. Johnson and R. W. Christy, "Optical constants of the noble metals," Phys. Rev. B **6**(12), 4370–4379 (1972).
17. O. Loebich, "The optical properties of gold," Gold Bull. **5**(1), 2–10 (1972).
18. V. Leroux and T. Eichner, "Github: spatio-temporal-couplings," https://github.com/VincentLeroux/spatio-temporal-couplings.
19. N. Delbos, C. Werle, I. Dornmair, T. Eichner, L. Hübner, S. Jalas, S. Jolly, M. Kirchen, V. Leroux, P. Messner, M. Schnepp, M. Trunk, P. Walker, P. Winkler, and A. Maier, "LUX: A laser-plasma driven undulator beamline," Nucl. Instrum. Methods Phys. Res., Sect. A **909**, 318–322 (2018).
20. S. Akturk, X. Gu, E. Zeek, and R. Trebino, "Pulse-front tilt caused by spatial and temporal chirp," Opt. Express **12**(19), 4399–4410 (2004).
21. Z. Li and J. Kawanaka, "Complex spatiotemporal coupling distortion pre-compensation with double-compressors for an ultra-intense femtosecond laser," Opt. Express **27**(18), 25172–25186 (2019).